Available online at www.sciencedirect.com
SCIENCE DIRECT®
Geochimica et Cosmochimica Acta 70 (2006) 101–117
Geochimica
www.elsevier.com/locate/gca

Alkenone paleothermometry: Biological lessons from marine sediment records off western South America

Fredrick G. Prahl *, Alan C. Mix, Margaret A. Sparrow

College of Oceanic and Atmospheric Sciences, Oregon State University, Corvallis, OR 97331-5503, USA

Received 14 March 2005; accepted in revised form 24 August 2005

Abstract

An empirical global core-top calibration that relates the alkenone unsaturation index $U^{K'}_{37}$ to mean annual SST (maSST) is statistically the same as that defined for a subarctic Pacific strain of *Emiliania huxleyi* (CCMP1742) grown exponentially in batch culture under isothermal conditions. Although both equations have been applied widely for paleoSST reconstruction, uncertainty still stems from two key ecological factors: variability in the details of biosynthesis among genetically distinct alkenone-producing strains, and impacts of non-thermal physiological growth factors on $U^{K'}_{37}$. New batch culture experiments with CCMP1742 here reveal that $U^{K'}_{37}$ diverge systematically from the core-top calibration in response to nutrient depletion and light deprivation, two physiological stresses experienced by phytoplankton populations in the real ocean. Other aspects of alkenone/alkenoate composition also respond to these stresses and may serve as signatures of such effects, providing an opportunity to detect, understand, and potentially correct for such impacts on the geologic record. A test case documents that sediments from the Southeast Pacific display the alkenone/alkenoate compositional signature characteristic of cells physiologically stressed by light deprivation. Such an observation could be explained if marine snow provided a major vector of sedimentation for these biomarkers. Late Pleistocene $U^{K'}_{37}$ records in the Southeast Pacific yield plausible paleotemperature histories of ice-age cooling, but ice-age alkenone/alkenoate signatures fall outside the range of modern calibration samples of similar $U^{K'}_{37}$. They better match core-top samples deposited beneath waters characterized by much cooler maSST, suggesting key features of ice-age ecology for alkenone-producing haptophytes were different from today, and that the $U^{K'}_{37}$ index taken alone may misgauge the total range of ice-age cooling at these locations. Analysis of the full spectrum of alkenone/alkenoate compositions preserved in sediments opens up a new opportunity that may improve the accuracy of paleotemperature estimates based on simple $U^{K'}_{37}$ analysis and help resolve longstanding disagreements between various paleotemperature reconstruction methods.

1. Introduction

Since publication of the seminal work by Brassell et al. (1986), the alkenone unsaturation index $U^{K'}_{37}$ has often been employed as a paleothermometric tool for Quaternary research. Establishment of a simple, statistically well-behaved global calibration (Muller et al., 1998) justifiably supports use of $U^{K'}_{37}$ as a proxy for reconstruction of mean annual sea-surface temperature (maSST). Nonetheless, paleoreconstructions of maSST change must still be scrutinized, as even small systematic biases can change inferences about mechanisms of climate change.

The relationship between $U^{K'}_{37}$ values and maSST is empirical (Herbert et al., 1998; Muller et al., 1998), not causative (e.g., Prahl et al., 2000). Sediment trap time series show that alkenone export from surface waters is seasonal in many ocean locations (see Prahl et al., 2000 and references therein). Also, the euphotic zone in many ocean locations is often thermally structured and modeled as a two-layered biological system (Coale and Bruland, 1987; Small et al., 1987). Thus, at least some portion of alkenone export could derive from deeper in the euphotic zone where temperatures are significantly colder than that at the sea surface (e.g., Bentaleb et al., 1999; Prahl et al., 1993, 2001; Ternois et al., 1997). Furthermore, work with laboratory cultures shows $U^{K'}_{37}$ values set by cells are species, even strain, dependent (e.g., Conte et al., 1998; Yamamoto

* Corresponding author. Fax: +1 541 737 2064.
E-mail address: fprahl@coas.oregonstate.edu (F.G. Prahl).

0016-7037/$ - see front matter © 2005 Elsevier Inc. All rights reserved.
doi:10.1016/j.gca.2005.08.023

et al., 2000), and are sensitive not only to growth temperature but also to physiological factors such as nutrient and light availability (e.g., Epstein et al., 1998, 2001). These observations contribute to uncertainty in absolute temperature estimates derived from $U^{K'}_{37}$ using a simple linear calibration curve, suggesting that the observed ±1.5 °C standard deviation of residuals in the global core-top calibration (compared to typical ±0.5 °C or better analytical reproducibility of single samples) reflects systematic ecological effects, rather than just random error. By better understanding how physiological factors act to shape the biochemical fingerprint, an opportunity is at hand to improve use of alkenones as paleotemperature proxies.

Here, we document concordance between maSST and $U^{K'}_{37}$ measured in modern sea-floor sediments accumulating along the continental margin, in deep basins, and on ridges off western South America, that is consistent with the previous global calibration (Muller et al., 1998). We also characterize the C_{37}, C_{38}, and C_{39} alkenone and related C_{36} alkenoate 'fingerprints' preserved in the surface sediments, and with depth in three piston cores from sites representative of the subpolar transition zone off southern Chile, the eastern boundary current off southern Peru, and the equatorial ''cold-tongue'' upwelling zone extending offshore from South America. Each of these piston cores yields perspective on glacial–interglacial changes in oceanographic conditions over the past ~150 Kyrs. Examination of our collective sediment data set in context with results from laboratory-controlled batch culture experiments shows that physiological factors likely have a significant impact on the biomarker signature (and the implied paleotemperature estimates) preserved in sediments from this region, and that key features of the ecology of alkenone producers were potentially quite different under ice-age conditions than at present, with no apparent modern analog in the region.

2. Materials and methods

2.1. Sediment samples

Near-surface sediment was sampled from 33 multicores collected in 1997 along a north-to-south transect from ~13 to 51°S off the Chile–Peru margin, and from four gravity and three piston cores collected along an east-to-west transect from ~90 to 140°W in the eastern equatorial Pacific. All multicores recovered pristine sediment–water interfaces, including soupy ''fluff'' layers. Upon recovery at sea, the multicores were stored vertically under refrigerated conditions (4 °C) in the Oregon State University (OSU) Core Repository (http://corelab-www.coas.oregonstate.edu/), and after several months of storage were split and described. These were then sealed in D-tubes and stored horizontally under refrigeration prior to sampling. The samples were taken in ~1 cm thick sections from within the bioturbated mixed-layer, as close to the core top as possible (Table 1). Samples taken at 5–6 cm depth in 13 of the multicores reflect the fact that sediments settled during vertical storage, and measurements of sample depths are indexed to the top of the liner; that is, the true depth of these samples below the original sediment–water interface is ~2–3 cm. Given the relatively high sedimentation rates in the region, in some cases of over 100 cm/kyr (Mix et al., 2003), all of these near-surface sediments are considered representative of modern conditions, averaged over the past few hundred to perhaps a thousand years because of bioturbation effects. Sediments were also sampled with depth in three piston cores: Y69-71P, Y71-6-12P, and RR9702A-11PC (Tables 1 and 2), which represent variations in composition over the last glacial–interglacial cycle.

2.2. Culture experiments

We selected a strain of *Emiliania huxleyi* (CCMP1742, aka 55a) (obtained from the Pravasoli-Guillard National Center for Culture of Marine Phytoplankton; http://ccmp.bigelow.org/) for culture experiments because its established $U^{K'}_{37}$-growth temperature calibration (Prahl et al., 1988) provides an excellent match with the empirical core-top calibration for $U^{K'}_{37}$ versus maSST (Muller et al., 1998).

Three manipulative batch culture experiments were conducted in controlled temperature baths using either f/2 or f/20 as the nutrient media (see CCMP website for recipes) and cool-white fluorescent lighting for illumination. Experiments were designed to allow daily sampling over a period extending from healthy, exponential growth into physiologically stressed growth. Inoculations used to initiate experiments were made using cell stocks acclimated previously for growth at the experimental temperature. In all experiments, cells were grown using a 12 h light/dark cycle. Light intensity during the day was held constant at ~50–60 μEin/(m^2 s). Each day, approximately 1 h after lights turned on automatically in the culture room, flasks were swirled gently to assure homogenization and immediately subsampled using a sterile pipette in order to monitor changes in alkenone/alkenoate content and composition, as well as cell density and nutrient concentration.

Cell density in the culture samples was determined microscopically using a hemocytometer. Cells for biomarker analysis were collected by filtration on pre-combusted (450 °C, 8 h) glass fiber filters (GF/F: 25 mm, Whatman), which were wrapped in aluminum foil and stored in an ultrafreezer (−80 °C) until needed. The filtrate from each subsample was collected in an acid-washed, plastic polyvial (30 mL) and stored frozen until analyzed for nitrate and phosphate by standard autoanalyzer techniques (Strickland and Parsons, 1972).

In one paired experiment, inoculated culture flasks (500 mL) containing f/20 media (~100 μM nitrate, 4 μM phosphate) were maintained isothermally at 15 °C and allowed to grow either exponentially until nutrient-depleted or until cell division was forced to stop by exclusion of all light. More details about this experimental design are given elsewhere (Prahl et al., 2003). This experiment evalu-

Table 1
Alkenone and other ancillary data for surface sediments collected along the continental margin off the west coast of South America

Code	Lat[a] (°S)	Long (°W)	Water depth (m)	sumSST[b] (°C)	winSST[b] (°C)	maSST[b] (°C)	Core depth (cm)[c]	OC (wt%)	%$CaCO_3$ (wt%)	ΣAlk[d] (μg/gOC)	$U^{K'}_{37}$	$U^{K'}_{37} - T$[e] (°C)	%K37[f]	%K38[f]	ME/K37[f]	EE/ME[f]
RR9702A-01MC3	50.7	77.0	3964	9.7	7.2	8.7	5.5	0.29	5.6	303	0.370	9.7	52	43	0.253	0.666
RR9702A-08MC2	46.4	76.7	3014	11.9	7.4	10.3	5.5	1.0	5.4	360	0.420	11.2	51	44	0.226	0.729
RR9702A-12MC2	43.4	76.3	3523	13.5	9.2	11.8	5.5	1.3	1.8	348	0.467	12.6	50	44	0.213	0.711
RR9702A-27MC2	40.5	75.9	3850	15.4	10.5	13.2	5.5	1.2	0.4	399	0.470	12.7	50	44	0.185	0.700
RR9702A-44MC2	35.8	73.0	172	16.3	10.7	13.6	5.5	2.5	3.3	294	0.488	13.2	53	43	0.183	0.653
RR9702A-50MC1	23.6	73.6	3396	20.4	16.0	17.8	5.5	0.27	63.4	169	0.640	17.7	53	42	0.118	0.780
RR9702A-60MC1	20.9	81.5	2480	21.4	18.0	19.4	5.5	0.2	90.5	78	0.707	19.7	[g]	[g]	[g]	[g]
RR9702A-34MC1	36.5	73.4	133	16.7	11.1	13.9	5.5	3.5	1.2	369	0.479	12.9	51	43	0.141	0.725
RR9702A-48MC3	32.6	73.7	3920	17.4	13.1	15.1	5.5	0.56	23.3	387	0.564	15.4	52	43	0.142	0.794
RR9702A-54MC1	21.4	81.4	1323	21.1	17.9	19.2	5.5	0.2	95.6	239	0.749	20.9	[g]	[g]	[g]	[g]
RR9702A-77MC1	16.1	77.0	2588	22.8	16.6	19.4	5.5	1.6	5.7	679	0.677	18.8	53	42	0.078	0.907
RR9702A-80MC4	13.5	76.9	448	21.7	14.7	18.0	5.5	4.4	0.3	657	0.699	19.4	55	42	0.060	0.779
RR9702A-31MC1	37.7	75.4	3946	17.0	11.7	14.3	5.5	1.3	0.4	505	0.495	13.4	49	45	0.160	0.751
RR9702A-06MC2	46.9	76.6	3298	11.9	7.4	10.3	0.5	0.89	2.7	376	0.402	10.7	47	48	0.239	0.684
RR9702A-14MC4	43.5	76.5	3471	13.5	9.2	11.8	0.5	1.1	1.6	354	0.453	12.2	47	47	0.202	0.711
RR9702A-20MC7	40.0	74.5	1055	15.9	10.1	13.2	1.5	1.0	4.5	452	0.479	12.9	47	48	0.186	0.710
RR9702A-04MC5	47.0	76.6	3354	11.9	7.4	10.3	2.5	0.92	2.7	399	0.410	10.9	46	48	0.241	0.717
RR9702A-10MC2	46.3	76.5	2879	11.9	7.4	10.3	2.0	0.85	6.5	398	0.430	11.5	47	47	0.232	0.696
RR9702A-22MC3	40.0	74.1	430	15.2	9.6	12.9	0.5	1.4	2.0	479	0.487	13.2	47	48	0.189	0.667
RR9702A-25MC2	39.9	75.9	4087	16.1	10.9	13.6	0.5	1.1	0.5	336	0.489	13.2	46	47	0.182	0.691
RR9702A-39MC3	36.2	73.6	510	16.7	11.1	13.9	2.0	2.3	1.0	392	0.507	13.8	49	46	0.174	0.697
RR9702A-42MC1	36.2	73.7	1028	16.7	11.1	13.9	0.5	2.4	4.7	441	0.481	13.0	50	46	0.186	0.668
RR9702A-46MC1	33.3	73.5	3852	16.9	12.6	14.7	2.0	0.94	7.8	397	0.533	14.5	49	46	0.170	0.740
RR9702A-52MC1	23.2	73.3	3418	20.4	16.0	17.8	2.5	0.33	54.2	167	0.633	17.5	51	45	0.125	0.729
RR9702A-62MC1	18.1	79.0	2937	22.5	17.6	19.7	1.5	0.92	75.7	68	0.698	19.4	53	44	0.106	0.889
RR9702A-72MC1	16.5	76.2	3782	22.8	16.6	19.4	2.0	0.84	0.5	349	0.696	19.3	52	44	0.083	0.869
RR9702A-74MC1	16.2	76.2	3476	22.8	16.6	19.4	2.0	1.2	0.1	478	0.675	18.7	53	44	0.088	0.982
RR9702A-66MC1	16.1	77.1	2575	22.9	16.9	19.6	2.0	1.6	6.4	427	0.677	18.8	53	44	0.095	0.819
RR9702A-68MC1	16.0	76.4	3228	22.8	16.6	19.4	1.5	1.6	0.0	513	0.685	19.0	51	45	0.077	0.886
RR9702A-70MC1	16.7	76.0	4124	22.8	16.6	19.4	3.0	0.67	0.0	270	0.661	18.3	53	43	0.098	0.894
RR9702A-64MC1	17.0	78.1	2930	22.9	17.4	19.8	2.0	0.44	55.9	227	0.701	19.5	52	44	0.086	0.982
RR9702A-83MC2	13.2	77.3	1419	22.3	15.9	18.9	2.5	8.9	0.0	571	0.748	20.9	52	44	0.070	0.890
RR9702A-82MC4	13.7	76.7	264	21.7	14.7	18.0	2.0	15.0	4.4	618	0.736	20.5	52	43	0.062	1.035
VNTR01-19PC	(7.9)	90.5	3448	27.6	26.8	27.4	3.5	[h]	[h]	[h]	0.911	25.6	[g]	[g]	[g]	[g]
VNTR01-9PC	3.0	110.5	3860	26.0	22.1	24.1	2.5	[h]	[h]	[h]	0.876	24.6	[g]	[g]	[g]	[g]
VNTR01-12GC	3.0	95.1	3535	26.3	20.3	23.2	3.5	[h]	[h]	[h]	0.802	22.4	[g]	[g]	[g]	[g]
VNTR01-10GC	4.5	102.0	3405	25.4	22.2	24.3	3.5	[h]	[h]	[h]	0.867	24.3	[g]	[g]	[g]	[g]
VNTR01-8PC	0.0	110.5	3791	25.7	21.8	23.4	0.5	[h]	[h]	[h]	0.868	24.4	[g]	[g]	[g]	[g]
VNTR01-21GC	(9.6)	94.6	3710	27.8	27.2	27.7	3.5	[h]	[h]	[h]	0.908	25.6	[g]	[g]	[g]	[g]
MANOP-14GC	(1.0)	140.0	3900	27.0	25.3	26.1	0.5	0.36	80	92	0.957	27.0	[g]	[g]	[g]	[g]

[a] Numbers in parentheses are north latitude, i.e. °N.
[b] sumSST, winSST, mast, summer, winter, and mean annual SST, respectively.
[c] Depths measured from top of core liner. Cores settled during transport, so all samples actually taken within the top 3 cm of original sediment–water interface.
[d] Total C_{37}, C_{38}, and C_{39} alkenone concentration.
[e] Temperature estimated from calibration equation $U^{K'}_{37} = 0.034T + 0.039$ (Prahl et al., 1988)
[f] Alkenone/alkenoate compositional properties—see text for definition.
[g] Chromatograms contained interfering peaks which prohibited reliable quantitation of these compositional properties.
[h] Not determined.

Table 2
Compositional data for alkenone/alkenoate signatures measured with depth in piston cores collected along the continental margin off the west coast of South America

RR9702A-11PC Latitude (46.317°S); Longitude (76.538°W); Water depth (2825 m)					Y71-6-12P Latitude (16.443°S); Longitude (77.563°W); Water depth (2734 m)							Y69-71P Latitude (0.083°N); Longitude (86.482°W); Water depth (2740 m)						
Depth (cm)	Age (Kyr)	$U^{K'}_{37}$	ME/K37	EE/ME	Depth (cm)	Age (Kyr)	$U^{K'}_{37}$	%K37	%K38	ME/K37	EE/ME	Depth (cm)	Age (Kyr)	$U^{K'}_{37}$	%K37	%K38	ME/K37	EE/ME
1.5	0.6	0.463	0.229	0.673	12.5	4.2	0.712	52	44	0.140	0.868	7.3	1.1	0.857	55	42	0.069	0.921
11.5	4.8	0.425	0.269	0.519	17.5	6.5	0.710	54	42	0.102	0.780	10.5	1.5	0.859	54	42	0.066	0.967
21.5	9.0	0.405	0.268	0.448	27.0	10.8	0.683	54	42	0.101	0.746	18.5	2.6	0.854	55	42	0.057	1.077
31.5	13.1	0.322	0.308	0.522	32.0	12.7	0.696	52	43	0.095	0.848	40.5	5.6	0.831	55	41	0.056	1.088
41.5	17.3	0.290	0.321	0.475	45.5	16.8	0.646	53	43	0.113	0.699	50.0	6.9	0.816	54	43	0.055	1.198
51.5	21.5	0.268	0.310	0.504	49.5	18.3	0.616	53	43	0.121	0.645	62.0	8.5	0.797	55	42	0.064	1.026
61.5		0.262	a	a	55.5	20.4	0.625	54	42	0.126	0.621	80.5	11.0	0.787	55	42	0.058	0.983
71.5		0.308	a	a	60.5	21.9	0.612	53	43	0.131	0.644	100.5	12.8	0.756	54	42	0.056	1.128
81.5		0.365	a	a	65.5	23.5	0.625	54	42	0.131	0.658	120.5	14.5	0.767	55	41	0.055	0.928
91.5		0.348	a	a	65.5	23.5	0.613	54	42	0.132	0.664	139.5	16.2	0.764	55	41	0.056	0.852
101.5		0.349	a	a	70.5	26.0	0.626	54	43	0.124	0.762	149.0	17.0	0.771	55	41	0.054	0.905
111.5		0.347	a	a	75.5	28.3	0.624	54	42	0.127	0.707	180.0	19.2	0.777	56	41	0.059	0.719
121.5		0.363	a	a	80.5	31.5	0.622	54	42	0.138	0.599	201.0	20.5	0.766	56	41	0.061	0.887
131.5		0.355	a	a	85.5	37.8	0.627	54	42	0.138	0.596	218.5	21.5	0.777	57	39	0.070	0.565
141.5		0.349	a	a	90.5	44.6	0.639	54	42	0.122	0.596	240.5	22.8	0.779	56	41	0.063	0.570
151.5		0.376	a	a	96.5	50.0	0.662	54	42	0.122	0.532	250.0	23.5	0.790	55	41	0.074	0.528
161.5		0.367	a	a	100.0	52.9	0.659	55	42	0.117	0.539	260.5	24.2	0.801	55	41	0.062	0.628
171.5		0.367	a	a	104.5	56.5	0.683	54	43	0.111	0.533	279.5	26.4	0.814	55	41	0.067	0.651
181.5		0.330	a	a	113.0	60.4	0.678	54	42	0.113	0.521	300.5	29.1	0.827	54	43	0.094	0.562
191.5		0.342	a	a	117.5	62.1	0.678	53	43	0.117	0.476	322.5	31.8	0.809	54	42	0.069	0.668
200.5		0.337	a	a	119.5	62.7	0.674	54	42	0.117	0.513	336.5	33.6	0.820	55	41	0.078	0.514
210.5		0.323	a	a	125.5	66.0	0.659	54	43	0.126	0.468	339.0	33.9	0.797	57	41	0.082	0.483
220.5		0.319	a	a	130.5	70.9	0.673	54	42	0.132	0.436	348.5	35.1	0.813	55	42	0.078	0.509
230.5		0.335	a	a	135.5	75.8	0.712	54	43	0.125	0.448	357.5	36.2	0.808	56	41	0.074	0.530
250.5		0.334	a	a	140.5	79.9	0.735	54	42	0.127	0.429	361.0	36.6	0.819	55	42	0.070	0.574
270.1		0.307	a	a	145.0	85.0	0.738	53	43	0.123	0.429	377.5	38.7	0.797	56	41	0.077	0.556
290.5		0.300	a	a	150.0	91.1	0.695	54	42	0.117	0.440	381.0	39.1	0.785	56	41	0.074	0.568
310.5		0.265	0.320	a	155.0	97.1	0.706	55	42	0.118	0.450	400.5	41.6	0.809	55	41	0.069	0.607
320.5		0.264	0.331	a	160.0	103.1	0.689	54	42	0.121	0.466	420.0	44.0	0.818	56	41	0.074	0.569
330.5		0.259	0.304	a	165.0	106.6	0.712	54	42	0.115	0.424	449.0	47.6	0.833	56	41	0.073	0.531
350.5		0.350	a	a	170.0	108.9	0.681	54	42	0.107	0.485	459.0	48.9	0.831	56	41	0.077	0.484
370.5		0.325	a	a	175.0	111.7	0.714	53	43	0.104	0.440	482.0	51.8	0.846	56	41	0.076	0.437
391.0		0.347	a	a	180.0	115.7	0.734	53	43	0.091	0.485	501.0	54.1	0.819	56	41	0.078	0.565
410.5		0.350	a	a	186.5	122.8	0.738	52	43	0.086	0.503	519.5	56.4	0.840	56	41	0.093	0.406
430.5		0.342	a	a	194.5	133.8	0.701	51	44	0.100	0.491	538.5	58.9	0.816	56	41	0.077	0.467
450.5		0.332	a	a	201.0	138.6	0.689	51	45	0.113	0.541	548.5	60.8	0.799	56	41	0.080	0.428
470.5		0.307	a	a	206.0	141.9	0.704	53	43	0.092	0.505	559.5	62.9	0.796	56	41	0.077	0.476
500.5		0.307	a	a	210.0	144.8	0.680	52	43	0.102	0.465	577.5	66.3	0.809	55	41	0.091	0.405
520.5		0.326	a	a	216.0	149.1	0.683	52	44	0.104	0.520	598.5	70.1	0.806	55	41	0.110	0.346
530.5		0.302	a	a	221.0	152.5	0.657	52	44	0.107	0.466	618.0	73.5	0.812	56	41	0.089	0.396
550.5		0.296	a	a	226.0	155.7	0.682	52	44	0.092	0.530	637.5	77.0	0.844	55	42	0.087	0.346
570.5		0.302	0.326	a	231.0	158.8	0.660	52	43	0.089	0.489	648.5	79.0	0.869	55	42	0.071	0.413
610.5		0.284	0.311	a	236.0	162.0	0.676	52	44	0.092	0.550	662.5	81.5	0.859	55	42	0.076	0.401
680.5		0.284	a	a	241.0	165.9	0.645	53	43	0.097	0.529	678.5	84.8	0.862	55	42	0.086	0.422
700.5		0.306	a	a	246.0	170.1	0.673	53	44	0.094	0.560	698.5	89.7	0.864	55	42	0.087	0.397

720.5		0.305	a		a	251.0		174.1		0.640	53		43	0.105		0.508	718.5	95.5	0.874	55	42	0.076	0.436
740.5		0.313	a		a												737.5	100.6	0.866	55	43	0.074	0.440
760.5		0.321	a		a												758.5	105.6	0.850	54	42	0.065	0.489
																	783.0	111.9	0.814	56	41	0.065	0.502
																	800.5	116.7	0.874	56	42	0.061	0.396
																	818.5	121.5	0.899	55	42	0.053	0.498
																	838.5	125.4	0.905	54	42	0.039	0.853
																	858.5	129.2	0.872	54	43	0.052	0.772
																	878.5	132.9	0.847	54	43	0.064	0.642
																	898.5	136.6	0.840	54	43	0.063	0.604
																	919.5	140.4	0.855	54	43	0.052	0.648
																	938.5	143.9	0.857	54	43	0.046	0.650
																	958.5	147.4	0.824	54	43	0.052	0.654
																	980.5	151.1	0.827	54	43	0.049	0.751
																	1002.5	155.0	0.843	54	43	0.046	0.819

a, Gas chromatographic interference prevented reliable quantitation.

ated how nutrient depletion, an environmental stress that would likely occur during termination of a bloom event, might affect the alkenone/alkenoate composition transmitted to the sediment record. In a second experiment, a pair of culture flasks was filled with f/2 media (~900 μM nitrate, 40 μM phosphate), inoculated, and allowed to grow exponentially for several days at 20 °C. Growth temperature was then abruptly decreased to 15 °C. When the 5 °C temperature decrease was imposed, one flask was covered for a continuous 5-day period with aluminum foil to exclude all light while the other, serving as a control, was left otherwise unchanged. This experiment was designed to evaluate the extent to which the alkenone/alkenoate composition of viable cells inadvertently packaged into settling materials such as marine snow could be modified physiologically during transit to the sediment record as viable cells experience temperature drop and complete darkness during settling. With the exception of higher nutrient concentrations and a temperature shift, this second experiment was conducted in a manner identical with the first set.

The cultures grown using f/2 media have initial nutrient concentrations significantly higher than typical oceanic values. We chose this condition, however, to obtain sufficient material to monitor in detail changes in alkenone/alkenoate content through the different stages of this experiment from exponential to stressed growth under conditions that approximate in key ways known real-world effects. Such physiological stress effects cannot be simulated using chemostats which, by design, focus on nutrient-limited, steady-state, exponential growth conditions (e.g., Popp et al., 1998). Given our prior findings that the direct effects of high nutrient concentration are negligible on $U^{K'}_{37}$ (Prahl et al., 1988), we believe the use in our culture experiments of a media with high initial nutrients is most appropriate.

2.3. Lipid biomarker analyses

Each sample, either as wet sediment (1–3 g dry) or as algal cells ($\geqslant 10^6$) on GF/F, was put into a glass centrifuge tube (50 mL), spiked with a recovery standard (nonadecan-2-one), and ultrasonically extracted using a 3:1 mixture of methylene chloride and methanol (20 mL, 3×). Extracts were combined in a separatory funnel and, after addition of pre-extracted water (10 mL), partitioned into hexane (20 mL, 3×). The hexane solution was then dried over granular, anhydrous Na_2SO_4 (24 h) and the solvent was subsequently removed by rotary evaporation under gentle vacuum at room temperature.

From the resultant lipid residue, a fraction enriched in C_{37}–C_{39} alkenones and C_{36} alkenoates (Brassell, 1993) was isolated by silica gel column chromatography. The concentration and composition of the alkenone/alkenoate mixtures contained in these fractions were measured quantitatively using on-column, capillary gas chromatography with flame ionization detection. See Prahl et al. (1989) for further procedural details. All reported concentration data

have been corrected for internal standard recovery, which was typically 80–90%. The routine precision on biomarker concentration and relative compositional properties and the unsaturation index $U^{K'}_{37}$ was typically better than ±5–10% and ±0.5–1%, respectively.

2.4. Elemental carbon analyses

Total carbon (TC) and total organic carbon (OC) were measured in all multicore samples by a high-temperature combustion method using a Carlo Erba NA-1500 Elemental Analyzer. Prior to elemental analysis, subsamples of sediment slotted for OC determination were treated with an excess quantity of a volatile acid (either concentrated HCl or H_2SO_3) to remove inorganic carbon (Hedges and Stern, 1984; Verardo et al., 1990). Calcium carbonate content of each sample was then estimated as a weight percentage of dry sediment (%$CaCO_3$), assuming all detectable inorganic carbon, calculated from the difference between TC and OC, exists in that mineralogical form.

2.5. Stable isotope analyses and chronostratigraphy

Stratigraphic and chronologic control in the sediment cores is provided by oxygen isotope analysis of the benthic foraminfera, *Uvigerina peregrina* and/or *Planulina wuellerstorfi*, using Finnigan MAT-251 and MAT-252 mass spectrometers at Oregon State University. Acid digestion of carbonate shells was done using an Autoprep Systems common acid batch system online with the MAT-251, or using a Finnigan "Kiel-III" separate acid bath device online with the MAT-252. Calibration to the widely accepted Pee Dee Belemnite (PDB) scale was accomplished by analysis of two standards from the National Institute of Standards and Technology (NIST): NBS-19 and NBS-20. The precision of replicate $\delta^{18}O$ analyses for both standards was ±0.06‰, with no significant offset between results on the two different instruments.

Age models in the sediment cores are based on correlation of down-core $\delta^{18}O$ variations with global reference records (e.g., Martinson et al., 1987; Pisias and Mix, 1997) and linear interpolation between discrete time horizons. Additional chronologic control comes from published radiocarbon dates that have been converted to calendar ages (Clark et al., 2004; Feldberg and Mix, 2003).

3. Results

3.1. Sediment analyses

Near-surface sediment samples from 33 multicores, four gravity cores, and three piston cores (Fig. 1) were analyzed for both the content and composition of C_{37}, C_{38}, and C_{39} alkenones and C_{36} alkenoates (Table 1). Both types of compounds, biomarkers unique to a small subset of haptophyte algae (Green and Leadbetter, 1994), were readily detected constituents of the solvent extractable lipid fraction isolated from all samples. The same compositional information was also obtained from analysis of sediments sampled stratigraphically in three piston cores (see stars in Fig. 1).

3.2. Alkenone content of surface sediments

Total alkenone concentrations (ΣAlk), defined by the sum of all di- and tri-unsaturated C_{37} methyl, C_{38} methyl and ethyl, and C_{39} ethyl ketone constituents (Brassell, 1993), spanned almost two orders of magnitude in the sample set, ranging from 0.1 to 92 μg/g dry sediment and averaging 8.0 μg/g. ΣAlk normalized to total organic carbon (OC) also spanned a wide range, from 68 to 679 μg/gOC. ΣAlk normalized to dry sediment weight covaries positively with the weight percent OC content of sediments (%OC) with a high degree of correlation ($r = +0.993$). Although this statistical finding supports the interpretation that the OC content of these sediments is predominantly of marine origin, such inference cannot be made unequivocally from simple correlation alone.

3.3. Calcium carbonate content of surface sediments

%$CaCO_3$ estimates varied widely in the set of surface sediments examined, from undetectable to ⩾95% (Table 1). Since the coccolithophorid *E. huxleyi* is considered a dominant source of alkenones in the world ocean today (Brassell, 1993), significant correlation between ΣAlk (normalized to dry sediment) and %$CaCO_3$ could be expected. These properties do covary positively, but the correlation is weak ($r = +0.26$). Additional $CaCO_3$ contribution from sources such as foraminiferal tests as well as fundamental differences in organic matter decomposition and $CaCO_3$ dissolution mechanisms probably account for this weak correlation.

3.4. Alkenone unsaturation pattern in surface sediments

$U^{K'}_{37}$ values measured in the set of surface sediments spanned ~60% of the 0 to 1 range possible for the index (Table 1). The correlation of $U^{K'}_{37}$ with SST in overlying surface waters (Table 1) is high regardless of whether World Ocean Atlas 2001 data (http://www.awi-bremerhaven.de/GEO/ODV/data/WOA01/) are viewed as summer (January–March: $r = +0.97$, $n = 40$), winter (July–September: $r = +0.96$) or mean annual ($r = +0.98$) values.

All $U^{K'}_{37}$ values were converted into algal growth temperature (gT) estimates using the established laboratory calibration equation for the benchmark strain of *E. huxleyi* CCMP1742 (i.e., $U^{K'}_{37} = 0.034T + 0.039$: Prahl et al., 1988). gT estimates ranged from 9.7 to 27 °C (Table 1), with values within the seasonal range of SST observed for waters overlying each coring site in all but two cases (VNTR01-19PC and 21GC) and generally approximating maSST. A scatter plot (Fig. 1) shows findings for surface sediments from our study region comply well with the $U^{K'}_{37}$–maSST calibration obtained by statistical analysis of the global data set (Muller et al., 1998).

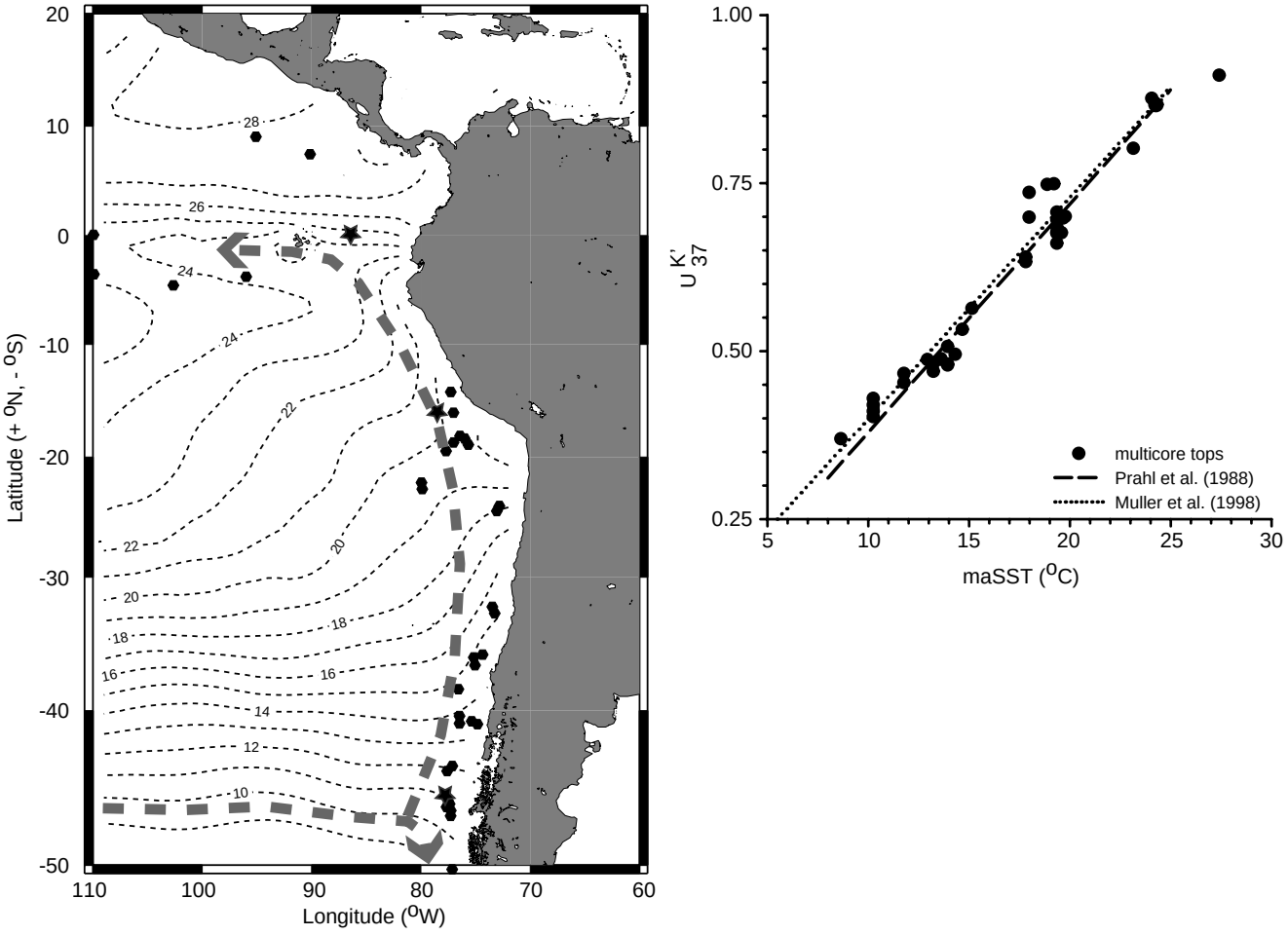

Fig. 1. Map on the left shows locations along the continental margin off the west coast of South America where sediment samples were obtained for detailed alkenone/alkenoate analysis. Solid symbols depict sites where surface sediments from core-tops were obtained from 33 multicores, three (of four) gravity cores, and three piston cores (Table 1); open stars depict three piston core sites where sediments were obtained stratigraphically with depth (Table 2). Dashed lines represent isotherms for mean annual sea-surface temperature (maSST) (Ocean Climate Laboratory, 2003). Major oceanographic currents and features in the study region (Strub et al., 1998) are also identified (bold arrows) to provide context for discussion. The graph on the right shows a scatter plot for $U^{K'}_{37}$ values measured in surface sediments versus maSST in waters overlying each multicore site (all data from Table 1). Dotted line depicts the global calibration equation ($U^{K'}_{37} = 0.033T + 0.044$) established for surface sediment collected from 60°N to 60°S throughout all ocean basins (Muller et al., 1998). Dashed line depicts the $U^{K'}_{37}$ versus temperature relationship established for a single strain of *E. huxleyi* grown in laboratory-controlled batch cultures ($U^{K'}_{37} = 0.034T + 0.039$: Prahl et al., 1988).

3.5. Alkenone/alkenoate signature in surface sediments

Four indices in addition to $U^{K'}_{37}$ describe the overall alkenone/alkenoate signature (Brassell, 1993) preserved in the surface sediments and its geographic variation throughout the study region (Table 1). Two indices (%K37, %K38) quantify the distribution of total C_{37} (or C_{38}) alkenones relative to alkenones of all three possible carbon chain lengths, i.e., C_{37}, C_{38}, and C_{39}. A third (ME/K37) quantifies the proportion of total C_{36} methyl ester (ME) concentration relative to total C_{37} alkenone (K37) concentration. And, a fourth (EE/ME) quantifies the distribution of the C_{36} alkenoate in its ethyl ester (EE) relative to its methyl ester (ME) form.

C_{37} components are the most abundant alkenones in all sediments, comprising 46–53% of the total. C_{38} components are next most abundant (43–48%), and C_{39} components are relatively rare (3–7%). Methyl esters of the C_{36} alkenoic acid are between ~5 and 25% as abundant as C_{37} alkenones. The relative proportion of the C_{36} alkenoic acid in its ethyl (EE) and methyl (ME) ester forms ranges from ~0.7–1.0.

Variations in %K37, ME/K37, and EE/ME in modern (core-top) sediments all follow systematic trends when plotted versus $U^{K'}_{37}$. %K37 values increase gradually in direct proportion to the alkenone unsaturation index (Fig. 2A) while ME/K37 values decrease (Fig. 2B). Although significant scatter masks any clear trend below a $U^{K'}_{37}$ of 0.6, an increase in EE/ME values is apparent for higher values of the alkenone unsaturation index (Fig. 2C).

3.6. Down-core stratigraphic biomarker distributions

Alkenone and alkenoate composition was also characterized stratigraphically with depth in cores collected at three specific locations along the continental margin off

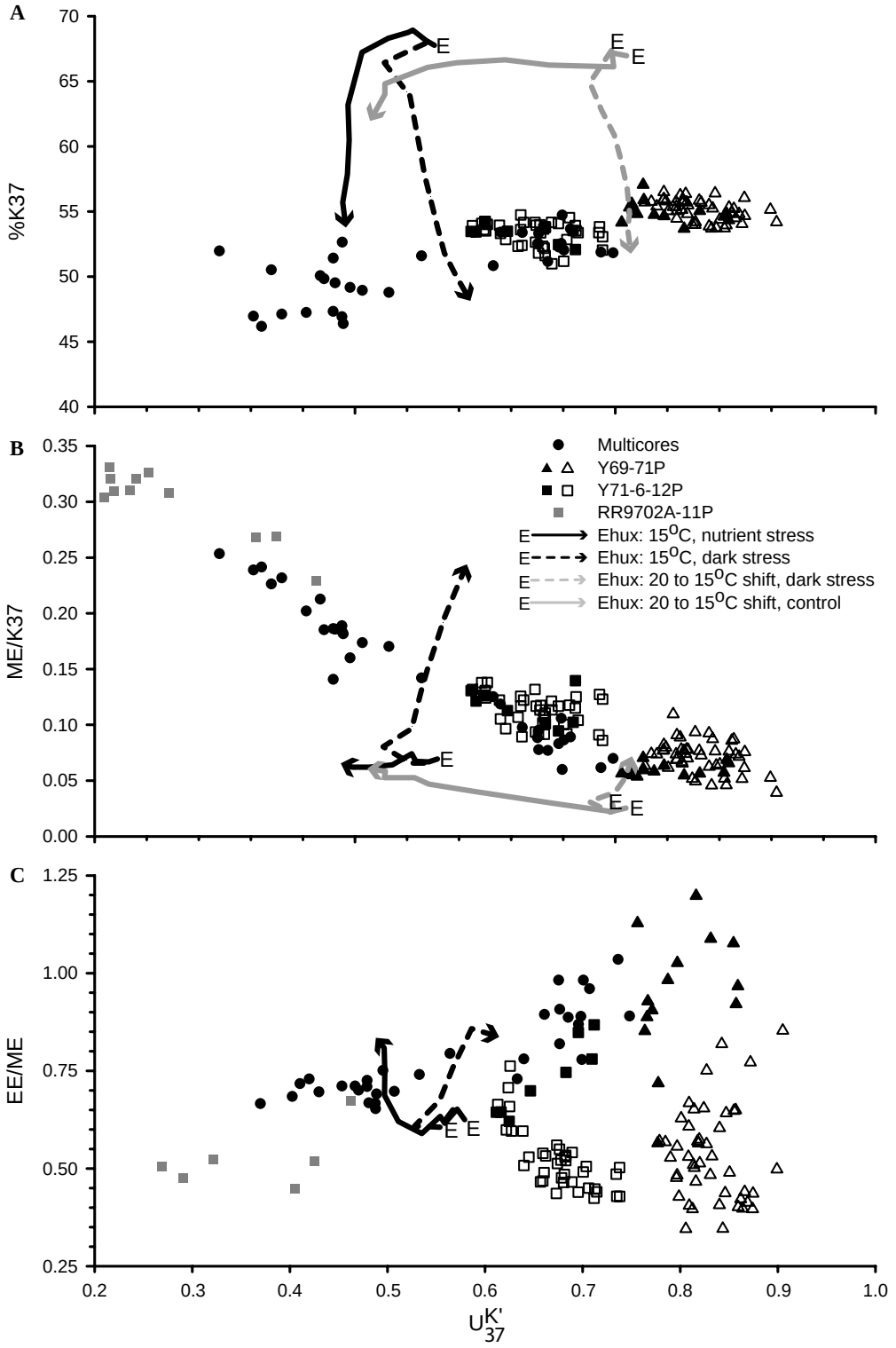

Fig. 2. Scatter plot of values for (A) %K37, (B) ME/K37, and (C) EE/ME versus $U^{K'}_{37}$ measured in surface sediments (Table 1) and three piston cores (Y69-71P, Y71-6-12P, and RR9702A-11PC: Table 2) from the continental margin off the west coast of South America (see text for definition of each compositional property). The black lines represent trends defined by data for the same compositional properties measured in a 'nutrient stress' (solid) and 'dark stress' (dashed) experiment with *E. huxleyi* grown isothermally at 15 °C under laboratory-controlled, batch culture conditions. The solid grey lines represent trends defined by time series data obtained from an experiment where 'dark stress' was imposed with a simultaneous 5 °C decrease in growth temperature (i.e., 20–15 °C). The dashed grey lines represent the trend for a control on the latter experiment, i.e., case where the 20–15 °C temperature shift was imposed with no dark stress. The letter E associated with each line depicts the composition of exponentially dividing cells at the start of each experiment. The arrowhead on each line indicates the time series trajectory of compositional change caused by each stress. All culture data used to draw the lines depicted in this figure are given in Table 3. The filled and open symbols for core data correspond to sediments deposited since and prior to the LGM (21 Ka), respectively.

the west coast of South America (Fig. 1). One (Y69-71P: 0.08°N, 86.5°W) records the depositional history of equatorial waters at the northern edge of our surface sediment survey area. The second (Y71-6-12P: 16.4°S, 77.6°W) records the depositional history of waters underlying a subtropical section of the Peru Current. And the third (RR9702A-11PC: 46.3°S, 76.5°W) records depositional history in the subpolar transition zone, where waters from the West Wind Drift bifurcate into the north-flowing Peru Current and the south-flowing Cape Horn Current. In cores Y69-71P and Y71-6-12P, approximately 150 Kyr of deposition are represented based on $\delta^{18}O$ stratigraphy. Because of the scarcity of calcareous fossils and unavailability of radiocarbon data, assignment of an equivalent age scale for RR9702A-11PC is not now possible. For this core, tentative assignment of climate events is made based on correlation of $U^{K'}_{37}$ variations here with the other sites.

$U^{K'}_{37}$ was reliably determined in all intervals sampled from the three cores. Values varied significantly in each, spanning a range from 0.756 to 0.905, 0.612 to 0.738, and 0.259 to 0.463, respectively (Table 2). Down-core variations generally track benthic foraminiferal records of $\delta^{18}O$ available for both Y69-71P and Y71-6-12P (Figs. 3A and B) with colder temperature estimates broadly corresponding to glacial intervals (relatively high $\delta^{18}O$ values). Assignment of the LGM time horizon in RR9702A-11PC is placed within the 50–60 cm depth interval of the core based solely on visual inspection of the $U^{K'}_{37}$ profile (Fig. 3C).

The correspondence of $U^{K'}_{37}$ temperature estimates with oxygen isotope stages in both Y69-71P and Y71-6-12P is imperfect. For example, warming associated with the last deglaciation appears to lag $\delta^{18}O$ changes at the equator (Core Y69-71P) but leads to $\delta^{18}O$ changes in Y71-6-12P. In contrast with the alkenone-based estimates, temperatures inferred at the equator and in core Y71-6-12P based on planktonic foraminiferal species assemblages (Feldberg and Mix, 2003) yield higher-amplitude temperature changes, and the equatorial zone appears to warm earlier during the deglaciation than the eastern boundary current (Fig. 3).

Reliable stratigraphic measurement of the four other compositional properties (%K37, %K38, ME/K37, and EE/ME) analyzed in surface sediments was only possible

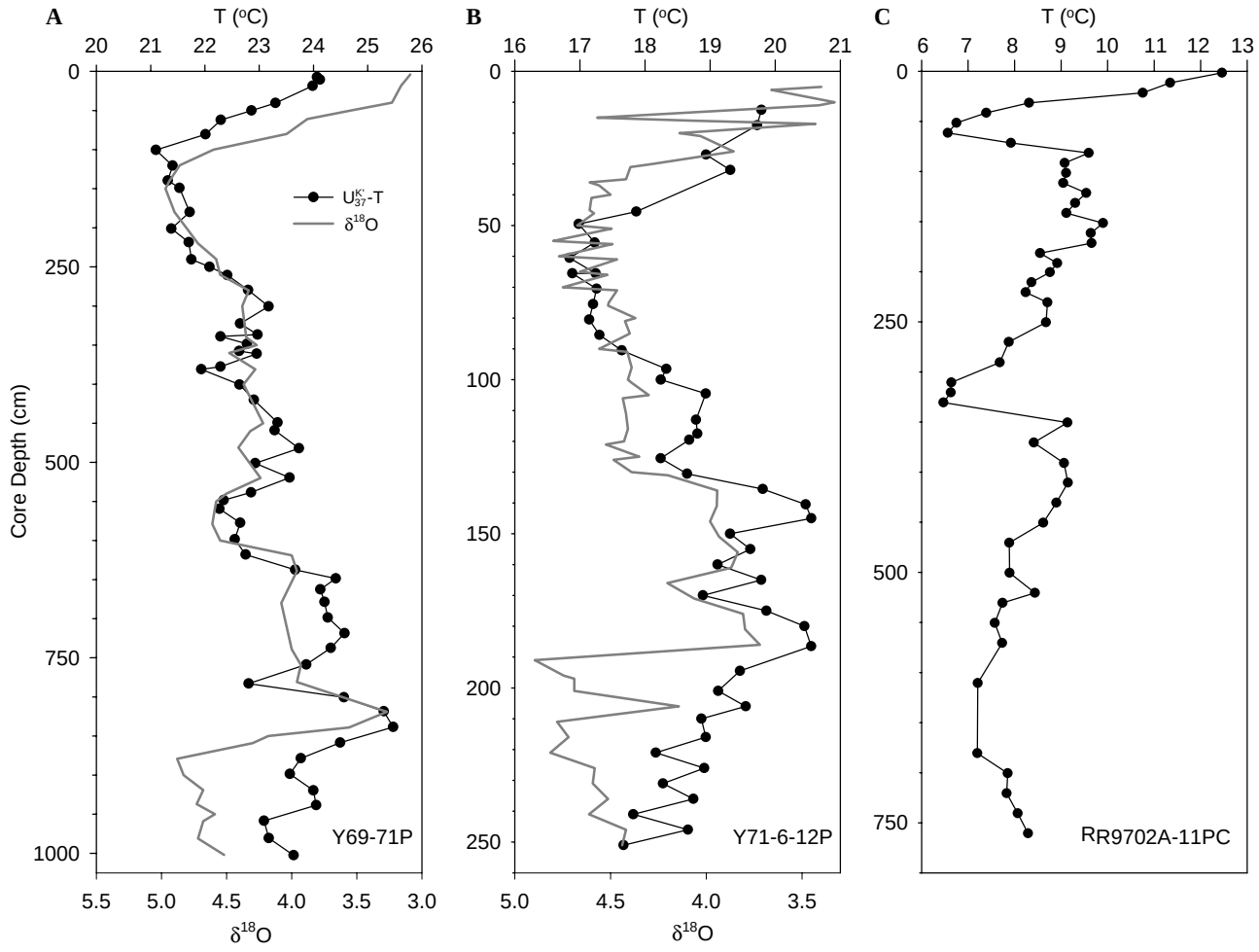

Fig. 3. Profiles for estimates of $U^{K'}_{37}$-based sea-surface temperature (SST) with depth in three piston cores from the study area (Fig. 1): (A) Y69-71P; (B) Y71-6-12P; and (C) RR9702A-11PC. SST estimates were calculated using a standard calibration equation ($U^{K'}_{37} = 0.034T + 0.039$: Prahl et al., 1988). The depth profile for stable oxygen isotope measurements ($\delta^{18}O$) on benthic foraminiferal tests from discrete depths in Y79-71P (Clark et al., 2004) and Y71-6-12P (Feldberg and Mix, 2003) are also plotted in (A) and (B) for stratigraphic reference purposes.

in Y69-71P and Y71-6-12P. Weak biomarker signal combined with the presence of interfering gas chromatographic peaks prevented their routine determination in RR9702A-11PC in all but a few cases for ME/K37 and EE/ME. Complete down-core records for %K37 and ME/K37 in Y69-71P and Y71-6-12P are plotted in Figs. 2A and B, respectively. In both cores, the signatures for these properties fall along trends defined by corresponding surface sediment data. GC traces were of sufficiently high quality in the case of only ~10% of the samples analyzed from R9702A-11PC to allow confident determination of ME/K37. All acceptable data from this core fall along the projected surface-sediment trend defined for this property (Fig. 2B).

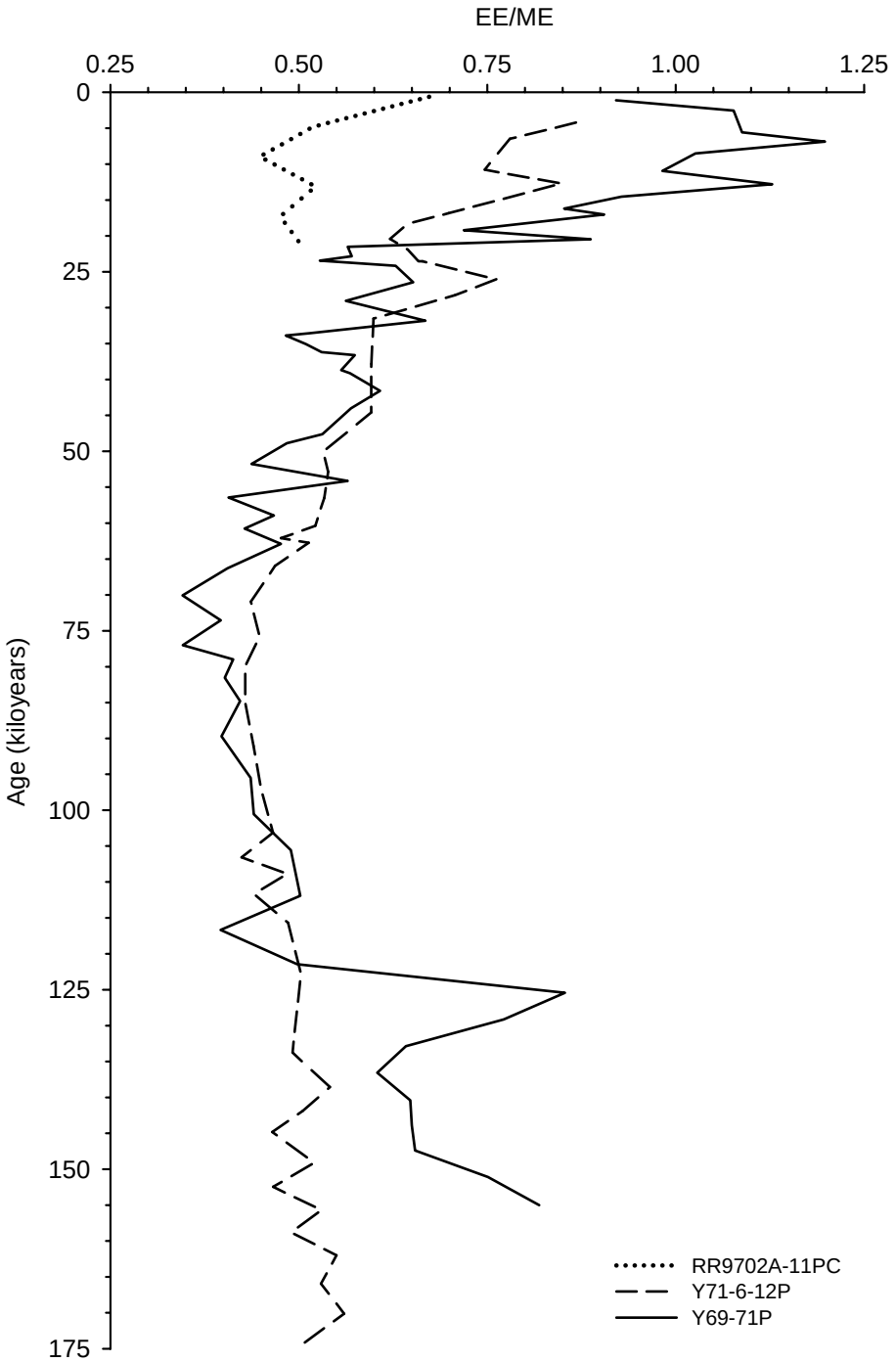

Fig. 4. Stratigraphic profiles for EE/ME values measured in three piston cores from our study area (Y69-71P; Y71-6-12P; and RR9702A-11PC, see stars in Fig. 1). An age model was established for the first two cores using available depth records for $\delta^{18}O$ in benthic foraminiferal shells and radiocarbon dates on foraminiferal carbonate in sediment samples from discrete depths (Pisias and Mix, 1997). For the third core, ages were assigned more arbitrarily, assuming a constant rate of sedimentation and the LGM time horizon (21 Kyr) corresponds to the depth of the observed $U^{K'}_{37}$ minimum at ~50 cm (Table 2).

In contrast to the case for %K37 and ME/K37, EE/ME from pre-Holocene samples for Y69-71P and Y71-6-12P deviate significantly from the surface-sediment trend (Fig. 2C). Closer examination shows that EE/ME varies systematically through time. EE/ME for all depth intervals younger than ~17 Kyr in Y69-71P and ~28 Kyr in Y71-6-12P are reasonably consistent with the surface-sediment trends, but decrease at greater ages, until returning to near-modern values in Y69-71P at ages >120 ka (Fig. 4). In RR9702A-11PC, GC data quality limited reliable EE/ME determination to only the six samples examined above the purported LGM depth at ~50–60 cm. Although the surface-sediment value is consistent with the regional trend for modern samples, EE/ME appears anomalously low (Fig. 2C). The shift to lower EE/ME values in RR9702A-11PC occurs at younger age than that observed in lower latitude cores Y71-6-12P and Y69-71P, in which EE/ME values display gradual increase beginning approximately at the depth of oxygen isotope stage boundary 3/2 and extending through the LGM to recent times (Fig. 4).

A long-term preservational effect provides one possible explanation for this EE/ME deviation in older sediments. That is, the ethyl ester (EE) may over long time spans be selectively degraded relative to its methyl ester (ME) form. However, EE/ME in Y69-71P returns down-core to values within the modern range of values (Fig. 4), arguing against accumulation of monotonic preservational effects over time.

An alternative possibility is that the assemblage of organisms contributing to this biomarker record has changed over time, i.e., there is no modern analog for alkenone producers present during some intervals of the last ice age. If so, this finding would challenge the accuracy of absolute ice-age temperatures derived from alkenones in this region. The relatively low EE/ME signatures in the ice-age samples are consistent with core-top samples associated with much lower maSST than is suggested by their $U^{K'}_{37}$ signature (Fig. 2). Clearly, we must better understand physiological controls on these changing biomarker compositions in order to assess unequivocally the implications for paleoceanographic reconstruction of surface water temperatures.

3.7. Physiological controls on biomarker composition

Results from a 'nutrient stress' and a 'dark stress' experiment (Table 3) confirm that the alkenone content of *E. huxleyi* can vary widely depending upon the cell's physiological status (Conte et al., 1998; Epstein et al., 1998). Significant increase in alkenone concentrations occurs under well-illuminated, nutrient-limited stationary growth conditions while significant decrease occurs when cells are exposed to prolonged darkness. Results also confirm that the metabolic gain and loss of cellular alkenone content can occur compound selectively and lead to considerable variation in $U^{K'}_{37}$ values independent of temperature. Selective mobilization of compounds has an opposite effect on $U^{K'}_{37}$, causing values to decrease under nutrient stress conditions and to increase in the case of prolonged dark stress. The magnitude of the impact on $U^{K'}_{37}$ values in the algal strain studied (CCMP1742) is equivalent to that expected for a growth temperature change of up to ±3 °C when gauged using the empirical relationship established from global surface sediments (Muller et al., 1998).

Tabulated results also show that non-thermal physiological factors can significantly impact compositional properties of the overall alkenone/alkenoate signature, not just the C_{37} alkenone unsaturation index $U^{K'}_{37}$. However, impacts of nutrient depletion and continuous darkness on the compositional properties %K37, ME/K37, and EE/ME are not opposite as observed for $U^{K'}_{37}$. At least in the paleoceanographic benchmark strain of *E. huxleyi*, CCMP1742, both effects are unidirectional for %K37, ME/K37, and nutrient stress has little quantitative effect on ME/K37.

Fig. 2 places collective compositional data obtained from these two batch culture experiments in quantitative perspective with sediment data. %K37, ME/K37, and EE/ME values measured in exponentially growing (i.e., unstressed) *E. huxleyi* cells all fall outside the compositional trend defined by sediment data, while those measured in cells exposed to longer periods of non-thermal stress tend toward the sediment recorded signature. The latter observation applies to all properties except ME/K37 in the case of the nutrient stress experiment. These findings imply that the alkenone/alkenoate signatures in these sedimentary records reflect the history of stressed populations, which may have relationships to the environment different from populations growing exponentially in continuous cultures. Of particular interest is our observation that populations stressed by nutrient deprivation may register paleotemperatures that are anomalously cold, or that populations stressed by light deprivation (e.g., in sinking blooms) may register paleotemperatures that are anomalously warm.

A 'dark stress' experiment analogous to the one just described, but with a 5 °C decrease in growth temperature (which simulates settling of viable phytoplankton out of the euphotic zone and into underlying, colder waters), yielded effects on the cellular biomarker content and the compositional properties of %K37, ME/K37, and EE/ME similar to those of the prior experiment (Table 3). There was one most notable exception, however—virtually no change in $U^{K'}_{37}$ values occurred. In this experiment, the decrease in growth temperature fortuitously compensated for the effect of prolonged darkness on $U^{K'}_{37}$ values. In a control for the latter 'dark stress' experiment, growth temperature was shifted but a normal daily 12 h L:D cycle was maintained. Control results revealed that $U^{K'}_{37}$ responds immediately to the shift in growth temperature, as expected from prior culture work (Prahl et al., 1988). %K37, ME/K37, and EE/ME values also all responded and displayed shifts in the direction expected for cells rapidly adapting to the new growth temperature (Fig. 2).

Overall findings demonstrate that the alkenone/alkenoate composition of *E. huxleyi* grown in culture can be affected significantly by temperature not only when these

Table 3
Summary of results from batch culture experiments with *E. huxleyi* strain CCMP1742

Sampling day	Growth condition	Density (cells/mL)	Nitrate (μM)	Phosphate (μM)	ΣAlk (pg/cell)	$U^{K'}_{37}$	%K37	%K38	ME/K37	EE/ME
Isothermal (15 °C), 'Nutrient Stress' Experiment										
1	15°, 12:12 L/D	1.93E+05	83.1	11.5	1.2	0.579	68	31	0.070	0.627
2	15°, 12:12 L/D	3.18E+05	74.3	10.7	1.2	0.572	68	31	0.068	0.652
3	15°, 12:12 L/D	4.27E+05	61.6	9.8	1.5	0.559	69	30	0.067	0.617
4	15°, 12:12 L/D	6.16E+05	44.5	8.5	1.3	0.554	69	30	0.073	0.635
5	15°, 12:12 L/D	9.39E+05	18.3	6.6	1.5	0.535	68	31	0.065	0.592
6	15°, 12:12 L/D	1.26E+06	0.1	4.5	1.4	0.511	67	31	0.061	0.621
7	15°, 12:12 L/D	1.48E+06	0.2	2.8	2.0	0.497	63	35	0.062	0.686
8	15°, 12:12 L/D	1.54E+06	0.2	1.6	2.7	0.498	61	37	0.063	0.721
9	15°, 12:12 L/D	1.60E+06	0.1	0.5	3.3	0.496	58	39	0.064	0.809
10	15°, 12:12 L/D	1.72E+06	0.0	0.5	3.3	0.492	56	41	0.063	0.820
11	15°, 12:12 L/D	1.76E+06	0.0	0.5	3.7	0.493	54	42	0.066	0.797
Isothermal (15 °C), 'Dark Stress' Experiment										
1	15°, 12:12 L/D	2.04E+05	81.9	11.4	1.5	0.566	68	31	0.066	0.650
2	15°, Dark Shift	3.06E+05	74.3	10.8	1.5	0.553	67	32	0.067	0.608
3	15°, 24 D	3.82E+05	71.4	10.5	1.3	0.528	66	32	0.081	0.610
4	15°, 24 D	4.00E+05	70.4	10.4	1.0	0.554	64	35	0.096	0.675
5	15°, 24 D	4.17E+05	65.5	10.2	0.6	0.567	58	40	0.144	0.760
6	15°, 24 D	4.02E+05	59.8	9.8	0.5	0.587	51	46	0.197	0.859
7	15°, 24 D	3.99E+05	52.4	9.3	0.4	0.608	49	48	0.244	0.841
20–15 °C Temperature Shift, 'Dark Stress' Experiment										
1	20°, 12:12 L/D	3.64E+05	898	37.4	1.4	0.761	67	31	0.025	a
2	T and Dark Shift	5.59E+05	924	36.0	1.3	0.745	67	31	0.022	a
3	15°, 24 D	5.54E+05	918	36.9	1.3	0.725	65	33	0.031	a
4	15°, 24 D	5.58E+05	924	37.0	0.95	0.749	61	37	0.040	a
5	15°, 24 D	5.41E+05	924	37.5	0.66	0.764	56	42	0.053	a
6	15°, 24 D	5.11E+05	922	37.1	0.62	0.763	54	44	0.063	a
7	15°, 24 D	5.29E+05	929	37.1	0.61	0.765	52	45	0.066	a
Control for 20–15 °C Temperature Shift, 'Dark Stress' Experiment										
1	20°, 12:12 L/D	1.41E+05	955	34.4	1.8	0.747	67	31	0.028	a
2	T Shift, 12:12 L/D	2.37E+05	790	28.6	1.5	0.749	66	32	0.023	a
3	15°, 12:12 L/D	2.83E+05	931	33.5	1.6	0.687	66	32	0.030	a
4	15°, 12:12 L/D	3.62E+05	924	32.5	1.8	0.645	67	32	0.036	a
5	15°, 12:12 L/D	5.52E+05	902	31.0	1.7	0.599	66	32	0.042	a
6	15°, 12:12 L/D	7.94E+05	871	28.8	1.8	0.571	66	32	0.048	a
7	15°, 12:12 L/D	9.73E+05	842	26.8	1.9	0.556	66	32	0.053	a
8	15°, 12:12 L/D	1.55E+06	749	22.4	2.1	0.529	65	33	0.053	a
9	15°, 12:12 L/D	1.92E+06	818	23.2	1.8	0.530	64	34	0.059	a
10	15°, 12:12 L/D	2.86E+06	679	15.9	1.6	0.517	62	35	0.060	a

a, Cannot be calculated; EE not resolved by GC from tri-unsaturated C_{38} ethyl ketone; hence, calculated %K37 and %K38 values are ~3% too low and too high, respectively.

biomarkers are biosynthetically assembled but also when they are metabolically destroyed by the cell. Assuming the noted compensatory effect of cooling on the $U^{K'}_{37}$ expressed by cells under prolonged darkness is applicable to populations growing in the real ocean, such effects might mitigate some apparent temperature biases depending on the sinking rate of cells relative to the thermal gradient experienced with depth.

4. Discussion

Paleoceanographers now employ a variety of methods to reconstruct glacial–interglacial sea-surface temperature (SST) change throughout different regions of the world ocean. The classic method for SST reconstruction, involving statistical analysis of microfossil species assemblages derived from planktonic organisms such as foraminifera, radiolaria, and diatoms (CLIMAP, 1981), has been advanced with a variety of statistical schemes, including updated transfer functions that circumvent faunal no-analog problems (Mix et al., 1999), several different modern analogous methods (Ortiz and Mix, 1997; Pflaumann et al., 1996; Waelbroeck et al., 1998), neural network pattern matching schemes (Malmgren and Nordlund, 1997), and correspondence analysis methods that consider multiple environmental parameters (Morey et al., 2005). In spite of these advances, legitimate questions remain about the accuracy of faunal temperature estimates based on statistical calibrations, in part because different statistical methods give slightly different temperature estimates in some

regions (e.g., Kucera et al., 2005). Examples of promising geochemical approaches for SST reconstruction include measurement of magnesium to calcium ratios in planktonic foraminiferal shells (Elderfield and Ganssen, 2000) and the alkenone unsaturation index $U^{K'}_{37}$ (Brassell et al., 1986). Paired use of techniques such as these, however, has in some cases yielded conflicting conclusions about the magnitude and timing of SST change (e.g., Niebler et al., 2003), suggesting that the geochemical methods need to be assessed for biases just as the faunal methods do.

As a case in point, Feldberg and Mix (2003) argued, based on results from statistical analysis of foraminiferal species assemblages, that equatorial waters in the Eastern Tropical Pacific Ocean (ETP) during the LGM were 3–5 °C colder than at present while those in the north-flowing Peru Current off southern Peru were 6–8 °C colder. Our stratigraphic analysis of $U^{K'}_{37}$ in a core from the ETP (Y69-71P) and from the Peru Current off southern Peru (Y71-6-12P) suggests the magnitude of SST cooling in the LGM was ~3 °C at both sites (Figs. 3A and B), and the cooling occurred at slightly different times. Can the noted differences in assessment be reconciled objectively? A definitive answer to this question is beyond the scope of the present study, but it is now possible to more objectively advance our sense of uncertainty in $U^{K'}_{37}$-based SST estimates for the Southeast Pacific region, given results from a detailed analysis of alkenone/alkenoate compositions preserved in these sediments coupled with findings from our laboratory-controlled batch culture experiments with *E. huxleyi*.

4.1. Oceanographic controls on the sedimentary biomarker signature

The greatest uncertainty in the $U^{K'}_{37}$ technique now appears to stem from yet limited knowledge of the ecology of alkenone producers in surface waters and of the biogeochemical processes controlling alkenone export production from the euphotic zone. Two key questions arise. First, what species contribute to the alkenone/alkenoate signature preserved in sediments and how does this assemblage change through space and time? Second, what is the physiological status of cells packaged into settling particulate material that ultimately forms the long-term sedimentary record?

Our study shows surface sediments accumulating all along the continental margin off the west coast of South America are consistent with the global $U^{K'}_{37}$–maSST calibration, both in trend and scatter (Fig. 1). On this basis, the overall alkenone/alkenoate composition in exponentially dividing cells of this algal strain would be expected to closely match that preserved in surface sediment from our study region. However, preserved compositions of %K37, ME/K37, and EE/ME more closely match those in nutrient and/or dark stressed cells than those in healthy, exponentially dividing cells (Fig. 2). This finding is not surprising because biogenic sedimentation is largely controlled by the settling of particle aggregates (McCave, 1975), which originate from surface waters as products of feeding processes (Turner, 2002). Fecal pellets and marine snow (Passow et al., 2001; Thornton, 2002) represent two distinct classes of such biogenic particle aggregates. Assuming diagenetic overprinting is an insignificant process, the alkenone/alkenoate signatures recorded by sediments accumulating at the seafloor should reflect that encoded into fecal pellets and marine snow at the time such particle aggregates are produced or perhaps shortly thereafter.

Bloom events, although particularly renowned in regions of divergence where upwelling occurs, are features common to most oceanic surface waters (Miller, 2004). The fate for most bloom-generated organic matter is to be grazed and remineralized within the euphotic zone. However, some fraction survives in situ destruction and becomes packaged during grazing and other feeding processes into aggregates that rapidly settle out of the euphotic zone, thereby contributing to export production (Turner, 2002). Compositional characteristics of alkenone/alkenoate signatures encoded within export production would depend upon when during blooms that cells are packaged into these aggregates and specifically how the packaging occurred.

Blooms represent periods of unbalanced primary production in surface waters and are terminated ultimately by nutrient depletion (Miller, 2004) with processes such as lysis, either massive viral or auto-induced (e.g., Bidle and Falkowski, 2004 and references therein) further facilitating the termination. Some of the alkenone/alkenoate content of export production from blooms certainly derives from direct grazing of 'nutrient-stressed' cells and thereby should carry the biomarker signature of such cells to the seafloor. A significant fraction of the biomarker signature exported from surface waters is potentially associated with living cells inadvertently incorporated into marine snow aggregates generated by other planktonic processes within the euphotic zone (e.g., Thornton, 2002; Turner, 2002). The alkenone/alkenoate signature initially imparted to marine snow by capture of a viable cell, regardless of its growth stage, could then be physiologically modified over a period of days as the aggregate settled out of the euphotic zone into darkness in transit to the seafloor. In this way, the sediment record would also inherit a signature for 'stressed' cells.

Literature supports our proposition that the alkenone/alkenoate composition preserved in marine sediments is shaped by that most characteristic of stressed cells. Conte et al. (1998) documented significant compositional change as cells shifted from the exponentially dividing to the stationary growth phase. Conte et al. (1995) also compared their laboratory results for ME/K37 with measurements for this property in samples of suspended particulate materials (SPM) collected from the euphotic zone in the North Atlantic and found values measured in SPM collected under non-bloom and late bloom conditions were typically consistent with those characteristic of cultures in a stationary growth phase. Nonetheless, 'stressed' signatures were

not always observed in their work. SPM collected during periods of bloom development in mesocosm experiments displayed ME/K37 values fitting expectation, i.e., those characteristic of healthy, exponentially dividing cells. Given the findings of Conte's research group and our current results, a resemblance of alkenone/alkenoate compositions in surface sediments throughout our study area and those in 'stressed' cells of *E. huxleyi* is reasonable (Fig. 2).

Grimalt et al. (2000) reviewed a body of evidence from field study and laboratory experiments that suggest $U^{K'}_{37}$ is insensitive to significant alteration once set biosynthetically within the phytoplankton cell. However, results from more recent, follow-up studies suggest otherwise (Marchand et al., 2005; Rontani et al., 2005). Diagenetic effects would likely be most pronounced on ME/K37, a property based on the relative abundance of two functionally distinct compound classes with potentially the greatest susceptibility to differential degradation (Harvey, 2000). Indeed, experimental results from laboratory-based studies with microbes spanning a range of metabolisms show alkenoates are degraded more rapidly than alkenones (Teece et al., 1998). However, assuming the order of diagenetic selectivity defined by these laboratory experiments applied to natural environments, diagenesis could not possibly transform the ME/K37 composition of healthy, exponentially dividing cells into one resembling that preserved in sediments from our study area, because the trend is opposite (Fig. 2B). Furthermore, field evidence is lacking for significant differential degradation of alkenones and alkenoates. In the North Atlantic, comparable rates of loss were apparent for both compound classes at five bathypelagic sediment sites (Madureira et al., 1995) and no significant offset was apparent between ME/K37 compositions in SPM and underlying sediment (Conte et al., 1995). On this basis, we discount diagenesis as a key cause for compositional differences noted between alkenone/alkenoate signatures in living cells of *E. huxleyi* and those preserved in sediments and submit that ecological and physiological processes operating in the upper ocean are the controlling factors.

4.2. Impact of sedimentation process on alkenone-based SST estimations

Alkenone/alkenoate signatures preserved in marine sediments from the Southeast Pacific suggest that the preserved record derives predominantly from physiologically 'stressed' cells. Given that stresses imposed experimentally on cultured cells are similar to those present in the natural world and cause significant systematic variability in $U^{K'}_{37}$ values at a specified growth temperature, it is reasonable to infer that some of the observed scatter in the global core-top calibration for $U^{K'}_{37}$ versus maSST is not just random analytical noise. Thus, greater caution is required whenever down-core $U^{K'}_{37}$ measurements are used to reconstruct absolute changes in maSST. This point is particularly relevant when assessments disagree significantly with those made through analysis of alternative paleoSST proxies, the circumstance now apparent in many regions, including those represented by two core sites (Y69-71P and Y71-6-12P) studied in the present work.

How accurately does standard use of alkenone paleothermometry constrain the magnitude of maSST change between the LGM and the present in our study area? The method could either systematically under-estimate or over-estimate actual SST change, given a relatively minor change in the mechanical details of marine snow-dominated sedimentation (Thornton, 2002; Turner, 2002) such as a simple shift in the timing of biomarker export from surface water blooms. Whether the assessment yielded an under-estimate or over-estimate would depend on how the minor ecological change related to the past versus present ocean.

Let us assume that CCMP1742, the strain of *E. huxleyi* we cultured, represents the average alkenone/alkenoate producer living in surface waters throughout our study area at least since the LGM. Also, let us assume results from our batch culture experiments accurately gauge how the conditions of nutrient depletion and continuous darkness would impact the alkenone/alkenoate composition of these organisms in their natural environment. Given only the occurrence of nutrient stress and current prospects for minimal impact from selective diagenetic alteration, a match between the ME/K37 composition of cells and that preserved in surface sediments could then not be made (Fig. 2B) unless most cells contributing to the biomarker signal experienced dark stress at some point in their depositional history.

Extrapolating from culture results, dark stress acting alone would cause an increase in $U^{K'}_{37}$ or a perceived 'warming.' However, waters underlying the euphotic zone become colder. Results from our temperature shift experiment (Table 3) indicate the water temperature decrease encountered beneath the euphotic zone may partially, perhaps even fully compensate for the apparent 'warming' effect of just dark stress. Consequently, the $U^{K'}_{37}$ signature initially incorporated within sinking marine snow could potentially retain an approximate record of changing sea-surface temperature, despite significant metabolic loss of the biomarker signal in the viable cell under continuous darkness conditions. Of our three piston core sites, the temperature gradient between the euphotic zone (nominally ~100 m) and 250 m depth is strongest at the equatorial site (~10 °C on an annual average), intermediate at the Peru site (~5 °C), and lowest at the subpolar transition site (~2 °C) as shown by data from World Ocean Atlas 2001 visualized using Ocean Data View. On this basis, we predict the net impact of temperature compensation on any dark stress effect would be greatest at the equatorial site. However, under conditions of sea-surface cooling during glacial episodes, reduced thermal gradients with depth could allow more of the dark stress effect to be expressed, resulting in a slight under-estimate of temperature changes by $U^{K'}_{37}$. Conversely, an increase in the vertical thermal gradient during cold

periods, driven by subsurface temperature changes, could cause $U^{K'}_{37}$ to over-estimate changes in temperature.

No matter how the process of dark stress specifically impacts the $U^{K'}_{37}$ of viable cells captured within sinking marine snow in natural settings on a quantitative basis, it is possible that, for a given water temperature, the value incorporated within marine snow would not necessarily always start out the same. The initial value would depend upon the physiological status of the cell captured by the sedimentary process. For example, assuming results from laboratory experiments with CCMP1742 extrapolate to the field (see Popp et al., 2005; Prahl et al., 2005), cells captured under nutrient-replete, mid-bloom conditions would display $U^{K'}_{37}$ values appearing somewhat 'warmer' than those captured under nutrient-depleted late-bloom conditions. In the case of our Southeast Pacific study area, glacial conditions were thought to be more highly productive (Mohtadi and Hebbeln, 2004). If so, and this productivity was associated with less nutrient stress on the populations during cold events, $U^{K'}_{37}$ values could conceivably under-estimate total temperature changes.

4.3. The paleoceanographic tally

Unquestionably, significant glacial–interglacial variability in $U^{K'}_{37}$ is apparent in down-core stratigraphic records at three distinct sites in our study area (Table 2). In each case, values display a relatively smooth decrease back to the LGM. Standard translation of these records into maSST estimates suggests the magnitude of LGM 'cooling' was not the same everywhere (Fig. 3). It was similar (~3 °C) at the equatorial site (Y69-71P) and the site within the northern part of the Peru Current (Y71-6-12P) but two times greater at the site (RR9702A-11PC) where the West Wind Drift bifurcates, ultimately forming the Peru Current (Fig. 1).

Results for Y71-6-12P agree with previous alkenone-based estimates in the region (TG7, Calvo et al., 2001). Nevertheless, in view of prospects we document for non-thermal physiological impacts on $U^{K'}_{37}$, and our inference based on ME/EE signatures that all ice-age samples from the region may have no modern ecological analogs, there is now legitimate reason to question the accuracy of LGM 'cooling' assessed by this method, which is much less than that inferred from foraminiferal species assemblages (Feldberg and Mix, 2003; Kucera et al., 2005) and somewhat less than that inferred from radiolarian species assemblages (Pisias and Mix, 1997). Furthermore, analysis of $\delta^{18}O$ and Mg/Ca data for foraminifera preserved in cores from the equatorial region represented by Y69-71P suggests LGM 'cooling' was much less than that suggested by any of the faunal estimates, and only ~50% of the $U^{K'}_{37}$-based assessment made here (Koutavas and Lynch-Stieglitz, 2003). Clearly, no consensus yet exists about the true magnitude of ice-age cooling in this region.

Discrepancies between SST assessments based on analysis of alkenones and foraminiferal species assemblages are not unique to our study. Niebler et al. (2003) recognized similar effects in their paleoceanographic study of the equatorial and south Atlantic and its associated eastern boundary current system, especially in upwelling systems. They ascribed the discrepancy to differences in the life history of alkenone producers and foraminifera but did not address the issue of physiological impacts on $U^{K'}_{37}$. In view of our findings, non-thermal physiological impacts on the phytoplankton producing these biomarkers may provide at least partial explanation for the discrepancy and need to be considered carefully.

Finding systematic stratigraphic changes in the ME/EE signature suggests major changes occurred in the phytoplankton ecology of surface waters overlying each of our core sites. This prospect may provide a logical explanation for some of the observed misfits between records for $U^{K'}_{37}$ and various other types of temperature proxies. However, all fault cannot and should not be cast on the $U^{K'}_{37}$ method as some level of systematic bias almost certainly applies as well to other biologically based proxy assessments. Unfortunately, there is yet insufficient information available both from culture experiments with alkenone producers and analysis of core records from our study area to determine more specifically what type of ecological change may have occurred. Pending further study, we cannot determine confidently how our evidence for ecological change impacts the accuracy of $U^{K'}_{37}$-based maSST assessments. Nonetheless, given EE/ME values display the smallest LGM—Modern change in RR9702A-11PC (Fig. 4), we now propose that non-thermal physiological effects on the accuracy of maSST assessments are lowest and perhaps unimportant in the southern part of our study area. The stratigraphic behavior of EE/ME values in the two northern cores suggests non-thermal physiological factors have not been constant since the LGM. Consequently, the accuracy of LGM 'cooling' in these regions currently warrants greatest suspicion.

By careful analysis of the full alkenone/alkenoate compositional suite preserved in sediments, understanding of both past temperature changes and other key elements of paleocirculation and ecosystems will be improved, yielding deeper insights into past and plausible future changes in the global system. Advancement in future development of the $U^{K'}_{37}$ paleothermometer will almost certainly require coordinated laboratory culture and natural surface water studies, and efforts made to put new biological discoveries in oceanographic context with the fossil sediment record for these biomarkers.

5. Conclusions

(1) The regional core-top calibration for $U^{K'}_{37}$ versus maSST in the modern Southeast Pacific closely matches the equivalent global core-top calibration of Muller et al. (1998).
(2) Batch culture experiments with the paleoceanographic benchmark strain of *E. huxleyi*, CCMP1742, demonstrate there can be significant non-thermal

physiological effects on $U^{K'}_{37}$ and the alkenone/alkenoate composition. A compelling, although yet unproven, argument can be made that these non-thermal physiological effects shape the overall biomarker signature preserved in Southeast Pacific sediments and likely elsewhere in the ocean.

(3) Analysis of sediment cores collected on the continental margin off the west coast of South America yields plausible regional histories of paleotemperature based on $U^{K'}_{37}$, but other aspects of the preserved alkenone/alkenoate signature imply that ice-age samples may have no modern ecological analog in the core-top calibration set. Further analysis of the complete set of alkenone/alkenoate compositional properties in sedimentary records, in the modern water column, and in carefully designed culture experiments should shed light on these ecological issues and eventually yield richer information about paleoceanographic change than is now possible through current use of just the $U^{K'}_{37}$ index.

Acknowledgments

We are thankful to Joe Jennings for all nutrient analyses, Dr. R. Schlitzer for making available a powerful way to visualize data from World Ocean Atlas 2001 using the software package Ocean Data View (http://www.awi-bremerhaven.de/GEO/ODV/), and two reviewers (Jean-François Rontani and one anonymous) for highly constructive comments on a prior version of this paper. We are also most grateful to the National Science Foundation funded Core Repository at Oregon State University for providing all sediment samples analyzed in this study and to the Ocean Sciences Division of NSF for all research support (OCE-9730376: both F.G.P. and A.C.M.; OCE-9986306 and 0350409: F.G.P.).

Associate Editor: H. Rodger Harvey

References

Bentaleb, I., Grimalt, J.O., Vidussi, F., Marty, J.-C., Martin, V., Denis, M., Hatte, C., Fontugne, M., 1999. The C_{37} alkenone record of seawater temperatures during seasonal thermocline stratification. *Marine Chemistry* **64**, 301–313.

Bidle, K.D., Falkowski, P.G., 2004. Cell death in planktonic photosynthetic microorganisms. *Nature Reviews* **2**, 643–655.

Brassell, S.C., 1993. Applications of biomarkers for delineating marine paleoclimatic fluctuations during the Pleistocene. In: Engel, M.H., Macko, S.A. (Eds.), *Organic Geochemistry Principles Applications*. Plenum Press, New York, pp. 699–738.

Brassell, S.C., Eglinton, G., Marlowe, I.T., Pflaumann, U., Sarnthein, M., 1986. Molecular stratigraphy: a new tool for climatic assessment. *Nature* **320**, 129–133.

Calvo, E., Pelejero, C., Herguera, J.C., Palanques, A., Grimalt, J.O., 2001. Insolation dependence of the southeastern Subtropical Pacific sea surface temperature over the last 400 kyrs. *Geophysical Research Letters* **28**, 2481–2484.

Clark, P.U., McCabe, A.M., Mix, A.C., Weaver, A.J., 2004. Rapid rise of sea level 19,000 years ago and its global implications. *Science* **304**, 1141–1144.

CLIMAP Project Members, 1981. *Seasonal Reconstructions of the Earth's Surface at the Last Glacial Maximum*.

Coale, K.H., Bruland, K.W., 1987. Oceanic stratified euphotic zone as elucidated by ^{234}Th:^{238}U disequilibria. *Limnology and Oceanography* **32**, 189–200.

Conte, M.H., Eglinton, G., Madureira, L.A.S., 1995. Origin and fate of organic biomarker compounds in the water column and sediments of the eastern North Atlantic. *Philosophical Transactions of the Royal Society of London B* **348**, 169–178.

Conte, M.H., Thompson, A., Lesley, D., Harris, R., 1998. Genetic and physiological influences on the alkenone/alkenoate versus growth temperature relationship in *Emiliania huxleyi* and *Gephyrocapsa oceanica*. *Geochimica et Cosmochimica Acta* **62**, 51–68.

Elderfield, H., Ganssen, G., 2000. Past temperature and δ^{18}O of surface ocean waters inferred from foraminferal Mg/Ca ratios. *Nature* **405**, 442–445.

Epstein, B.L., d'Hondt, S., Hargraves, P.E., 2001. The possible metabolic role of C_{37} alkenones in *Emiliania huxleyi*. *Organic Geochemistry* **32**, 867–875.

Epstein, B.L., d'Hondt, S., Quinn, J.G., Zhang, J., Hargraves, P.E., 1998. An effect of dissolved nutrient concentrations on alkenone-based temperature estimates. *Paleoceanography* **13**, 122–126.

Feldberg, M.J., Mix, A.C., 2003. Planktonic foraminifera, sea surface temperatures, and mechanisms of oceanic change in the Peru and south equatorial currents, 0–150 ka BP. *Paleoceanography* **18**, 1016. doi:10.1029/2001PA000740.

Green, J.C., Leadbetter, B.S.C., 1994. *The Haptophyte Algae*. Clarendon Press, Oxford.

Grimalt, J.O., Rullkotter, J., Sicre, M.-A., Summons, R., Farrington, J., Harvey, H.R., Goni, M., Sawada, K., 2000. Modifications of the C_{37} alkenone and alkenoate composition in the water column and sediment: possible implications for sea surface temperature estimates in paleoceanography. *Geochemistry, Geophysics and Geosystems* **1**, 2000GC000053.

Harvey, H.R., 2000. Alteration processes of alkenones and related lipids in water columns and sediments. *Geochemistry, Geophysics and Geosystems* **1**, 2000GC000054.

Hedges, J.I., Stern, J.H., 1984. Carbon and nitrogen determinations of carbonate-containing solids. *Limnology and Oceanography* **29**, 663–666.

Herbert, T.D., Schuffert, J.D., Thomas, D., Lange, C., Weinheimer, A., Peleo-Alampay, A., Herguera, J.-C., 1998. Depth and seasonality of alkenone production along the California margin inferred from a core top transect. *Paleoceanography* **13**, 263–271.

Koutavas, A., Lynch-Stieglitz, J., 2003. Glacial–interglacial dynamics of the eastern equatorial Pacific cold tongue—Intertropical Convergence Zone system reconstructed from oxygen isotope records. *Paleoceanography* **18**, 1089. doi:10.1029/2003PA000894.

Kucera, M., Kiefer, T., Pflaumann, U., Hayes, A., Weinelt, M., Chen, M.-T., Mix, A.C., Cortijo, E., Duprat, J., Waelbroeck, C., 2005. Reconstruction of the glacial Atlantic and Pacific sea-surface temperatures from assemblages of planktonic foraminifera: multi-technique approach based on geographically constrained calibration datasets. *Quaternary Science Reviews* **24**, 951–998.

Madureira, L.A.S., Conte, M.H., Eglinton, G., 1995. The early diagenesis of lipid biomarker compounds in North Atlantic sediments. *Paleoceanography* **10**, 627–642.

Malmgren, B.A., Nordlund, U., 1997. Application of artificial neural networks to paleoceanographic data. *Palaeogeography, Palaeoclimatology, Palaeoecology* **136**, 359–373.

Marchand, D., Marty, J.-C., Miquel, J.-C., Rontani, J.-F., 2005. Lipids and their oxidation products as biomarkers for carbon cycling in the northwestern Mediterranean Sea: results from a sediment trap study. *Marine Chemistry* **95**, 129–147.

Martinson, D., Pisias, N.G., Hays, J.D., Imbrie, J., Moore, T.C.J., Shackleton, N.J., 1987. Age dating and orbital theory of the ice ages:

development of a high-resolution 0 to 300,000 year chronostratigraphy. *Quaternary Research* **27**, 1–27.

McCave, I.N., 1975. Vertical flux of particles in the ocean. *Deep-sea Research I* **22**, 491–502.

Miller, C.B., 2004. *Biological Oceanography*. Blackwell Science, Oxford.

Mix, A.C., Morey, A.E., Pisias, N.G., Hostetler, S.W., 1999. Foraminiferal faunal estimates of paleotemperature: circumventing the no-analog problem yields cool ice-age tropics. *Paleoceanography* **14**, 350–359.

Mix, A.C., Tiedemann, R., Blum, P. (Eds.), 2003. *Proc. ODP*, Initial Reports, 202, College Station, TX (Ocean Drilling Program).

Mohtadi, M., Hebbeln, D., 2004. Mechanisms and variations of the paleoproductivity off northern Chile (24°S–33°S) during the last 40,000 years. *Paleoceanography*, 19. doi:10.1029/2004PA001003.

Morey, A.E., Mix, A.C., Pisias, N.G., 2005. Foraminiferal assemblages preserved in surface sediments correspond to multiple environmental variables. *Quaternary Science Reviews* **24**, 925–950.

Muller, P.J., Kirst, G., Ruhland, G., von Storch, I., Rosell-Mele, A., 1998. Calibration of the alkenone paleotemperature index $U^{K'}_{37}$ based on core-tops from the eastern South Atlantic and the global ocean (60°N–60°S). *Geochimica et Cosmochimica Acta* **62**, 1757–1772.

Niebler, H.-S., Arz, H.W., Donner, B., Mulitza, S., Patzold, J., Wefer, G., 2003. Sea surface temperatures in the equatorial and South Atlantic Ocean during the Last Glacial Maximum (23–19 ka). *Paleoceanography* **18**, 1069. doi:10.1029/2003PA000902.

Ocean Climate Laboratory, 1999. World Ocean Atlas 1998. In: National Oceanographic Data Center (ed. 15).

Ortiz, J.D., Mix, A.C., 1997. Comparison of Imbrie-Kipp transfer function and modern analog temperature estimates using sediment trap and core top foraminiferal faunas. *Paleoceanography* **12**, 175–190.

Passow, U., Shipe, R.F., Murray, A., Pak, D.K., Brzezinski, M.A., Alldredge, A.L., 2001. The origin of transparent exopolymer particles (TEP) and their role in the sedimentation of particulate matter. *Continental Shelf Research* **21**, 327–346.

Pflaumann, U., Duprat, J., Pujol, C., Labracherie, L., 1996. SIMMAX: a modern analog technique to deduce Atlantic sea surface temperatures from planktonic foraminifera in deep-sea sediments. *Paleoceanography* **11**, 15–35.

Pisias, N.G., Mix, A.C., 1997. Spatial and temporal oceanographic variability of the eastern equatorial Pacific during the late Pleistocene: evidence from radiolarian microfossils. *Paleoceanography* **12**, 381–393.

Popp, B.N., Kenig, F., Wakeham, S.G., Laws, E.A., Bidigare, R.R., 1998. Does growth rate affect ketone unsaturation and intracellular carbon isotopic variability in *Emiliania huxleyi*. *Paleoceanography* **13**, 35–41.

Popp, B.N., Prahl, F.G., Wallsgrove, R.J., Tanimoto, J., 2005. Seasonal patterns of alkenone production in the subtropical oligotrophic North Pacific. *Paleoceanography*, in press.

Prahl, F.G., Collier, R.B., Dymond, J., Lyle, M., Sparrow, M.A., 1993. A biomarker perspective on prymnesiophyte productivity in the northeast Pacific Ocean. *Deep-sea Research I* **40**, 2061–2076.

Prahl, F.G., Herbert, T., Brassell, S.C., Ohkouchi, N., Pagani, M., Repeta, D., Rosell-Mele, A., Sikes, E., 2000. Status of alkenone paleothermometer calibration: report from Working Group3. *Geochemistry, Geophysics and Geosystems* **1**, 1–13.

Prahl, F.G., Muehlhausen, L.A., Lyle, M., 1989. An organic geochemical assessment of oceanographic conditions at MANOP Site C over the past 26,000 years. *Paleoceanography* **4**, 495–510.

Prahl, F.G., Muehlhausen, L.A., Zahnle, D.L., 1988. Further evaluation of long-chain alkenones as indicators of paleoceanographic conditions. *Geochimica et Cosmochimica Acta* **52**, 2303–2310.

Prahl, F.G., Pilskaln, C.H., Sparrow, M.A., 2001. Seasonal record for alkenones in sedimentary particles from the Gulf of Maine. *Deep-sea Research I* **48**, 515–528.

Prahl, F.G., Popp, B.N., Karl, D.M., Sparrow, M.A., 2005. Ecology and biogeochemistry of alkenone production at Station ALOHA. *Deep-sea Research I* **52**, 699–719.

Prahl, F.G., Wolfe, G.V., Sparrow, M.A., 2003. Physiological impacts on alkenone paleothermometry. *Paleoceanography* **18**, 1025. doi:10.1029/2002PA000803.

Rontani, J.-F., Bonin, P., Jameson, I., Volkman, J.K., 2005. Degradation of alkenones and related compounds during oxic and anoxic incubation of the marine haptophyte *Emiliania huxleyi* with bacterial consortia isolated from microbial mats from the Camargue, France. *Organic Geochemistry* **36**, 603–618.

Small, L.F., Knauer, G.A., Tuel, M.D., 1987. The role of sinking fecal pellets in stratified euphotic zones. *Deep-sea Research I* **34**, 1705–1712.

Strickland, J.D.H., Parsons, T.R., 1972. *A Practical Handbook of Seawater Analysis*. Fisheries Research Board of Canada.

Strub, T.P., Mesias, J.M., Montecino, V., Rutllant, J., Salinas, S., 1998. Coastal ocean circulation off western South America. In: Robinson, A.R., Brink, K.H. (Eds.), *The Sea*, vol. 11. John Wiley and Sons, New York, pp. 273–313.

Teece, M.A., Getliff, J.M., Leftley, J.W., Parkes, R.J., Maxwell, J.R., 1998. Microbial degradation of the marine prymnesiophyte *Emiliania huxleyi* under oxic and anoxic conditions as a model for early diagenesis: long chain alkadienes, alkenones and alkyl alkenoates. *Organic Geochemistry* **29**, 863–880.

Ternois, Y., Sicre, M.-A., Boireau, A., Conte, M.H., Eglinton, G., 1997. Evaluation of long-chain alkenones as paleo-temperature indicators in the Mediterranean Sea. *Deep-sea Research I* **44**, 271–286.

Thornton, D.C.O., 2002. Diatom aggregation in the sea: mechanisms and ecological implications. *European Journal of Phycology* **37**, 149–167.

Turner, J.T., 2002. Zooplankton fecal pellets, marine snow and sinking phytoplankton blooms. *Aquatic Microbial Ecology* **27**, 57–102.

Verardo, D.J., Froelich, P.N., McIntyre, A., 1990. Determination of organic carbon and nitrogen in marine sediments using the Carlo Erba NA-1500 analyzer. *Deep-sea Research I* **37**, 157–165.

Waelbroeck, C.L., Labeyrie, L., Duplessy, J.-C., Guiot, J., Labracherie, M., Leclaire, H., Duprat, J., 1998. Improving past sea surface temperature estimates based on planktonic fossil faunas. *Paleoceanography* **12**, 272–283.

Yamamoto, M., Shiraiwa, Y., Inouye, I., 2000. Physiological responses of lipids in *Emiliania huxleyi* and *Gephyrocapsa oceanica* (Haptophyceae) to growth status and their implications for alkenone paleothermometry. *Organic Geochemistry* **31**, 799–811.